Journal of Thermal Analysis, Vol. 46 (1996) 853-869

Dedicated to Professor Bernhard Wunderlich on the occasion of his 65th birthday

THERMAL ANALYSIS VIA MOLECULAR DYNAMICS SIMULATION

S. N. Kreitmeier[1], *G. L. Liang*[2], *D. W. Noid and B. G. Sumpter*

The University of Tennessee, Department of Chemistry, Knoxville, TN 37996-1600 and the Chemical and Analytical Sciences Division, Oak Ridge National Laboratory, Oak Ridge, TN 37831-6197, USA

Abstract

Thermal analysis by classical molecular dynamics simulations is discussed on hand of heat capacity of crystals of 9600 atoms. The differences between quantum mechanical and classical mechanical calculations are shown. Anharmonicity is proven to be an important factor. Finally, it is found that defects contribute to an increase in heat capacity before melting. The energy of conformational gauche defects within the crystal is only about 10% due to internal rotation. The other energy must be generated by cooperative strain. The conclusion is that the next generation of faster computers may permit wider use of molecular dynamics simulations in support of the interpretation of thermal analysis.

Keywords: anharmonicity, computer simulations, crystal, gauche defects, heat capacity, molecular dynamics, paraffin, polyethylene, thermal analysis

Introduction

In the past, nature was either studied by experiment or through theory. In the last two decades a third method evolved, the simulation using computers. Being neither theory nor experiment, it nevertheless provides an interesting base for the understanding of many physical problems that are too complicated to be solved analytically, and are too globally treated in experiments. Three major simulation techniques are nowadays used in polymer science. Molecular mechanics and energy minimizations [1, 2 and others] can lead to solutions of static problems and molecular conformations. In Monte Carlo methods [3–6 and others] the problem is normally abstracted and fundamental properties like scaling behavior are derived. In molecular dynamics methods, finally, [7–12

1 Present address: Universität Regensburg, Institut für Experimentelle und Angewandte Physik, Polymerphysik, D-93040 Regensburg, Germany

2 Present address: University of California, Department of Chemistry, Berkeley, CA 94720, USA

0368–4466/96/ $ 5.00

© 1996 Akadémiai Kiadó, Budapest

John Wiley & Sons, Limited
Chichester

and others] one makes use of solutions of the Newtonian equations. In a short time regime (up to nanoseconds) a relatively close relation to physical parameters is possible by the latter method.

Thermal analysis is based on measurements of heat capacity, heats of transition, or heats of reaction. All of these are well understood in terms of their molecular origin. It should thus be possible to simulate thermal analyses on computers. Although at present rather large computer resources are necessary to approach sample sizes unaffected by microscopic fluctuations and surfaces, extrapolating the enormous advance of computer capacity in recent years, it may not be long that thermal analysis equipment may be replaced by a computer. Our present thermal analysis simulator was a CRAY-XMP supercomputer needing the order of magnitude of hours to establish thermal equilibrium for a $2 \cdot 10^{-19}$ g sample.

In the present analysis the molecular dynamics simulation is based on classical mechanics. This implies certain restrictions in the interpretation of thermodynamic data, especially at lower temperatures. In this paper we will discuss heat capacity, which can be deduced from molecular dynamics simulations, its validity and some limiting factors.

Model

The data for the 'thermal analysis' were extracted from earlier reported computer simulations of paraffin/polyethylene using a united atom model [13, 14]. The CH_2 group was collapsed to an atom of mass $m=14.03$ Da. Each crystal consisted of 192 chains, each chain of 50 united atoms, the total number of atoms thus being 9600. In this paper the discussed initial structure is orthorhombic with the lattice parameters $a=0.74$, $b=0.49$, $c=0.25$ nm [15], c being the chain axis. The size of the crystals is about $6 \cdot 6 \cdot 6.3$ nm^3. The crystals were unconstrained, in contrast to other simulations [11, 16, 17]. The system can be thought of being a microcanonical assembly at zero pressure in vacuum. No boundary conditions were used. The cross-section of the crystal in its initial state is given in Fig. 1.

For the MD technique the following Lagrangian was taken

$$L = \frac{1}{2} m \sum_{i=1}^{N} (\dot{x}_i^2 + \dot{y}_i^2 + \dot{z}_i^2) \tag{1}$$

$$- \sum_{i=1}^{N-1} D(1 - e^{-\alpha (r_{i,i+1} - r_e)})^2 \tag{2}$$

$$- \sum_{i=1}^{N-2} \frac{1}{2} K_\Theta (\cos\Theta_{i,i+1,i+2} - \cos\Theta_o)^2 \tag{3}$$

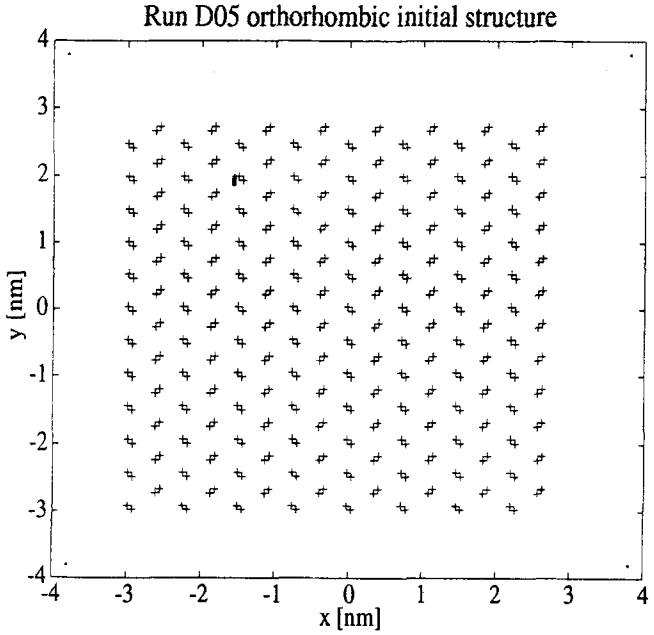

Fig. 1 Initial structure of the orthorhombic crystal in *x*-*y* projection (along the chain axis)

$$-\sum_{i=1}^{N-3}(8.37 - a\cos\tau_{i,i+1,i+2,i+3} + b\cos\tau^3_{i,i+1,i+2,i+3}) \tag{4}$$

$$-\sum_{|i-j|\geq 4}^{N} 4\varepsilon\left(\left(\frac{\sigma}{r_{ij}}\right)^{12} - \left(\frac{\sigma}{r_{ij}}\right)^{6}\right) \tag{5}$$

The term (1) is the kinetic energy, followed by the potential energy terms (2)–(5). The second term represents the stretching vibrations of adjacent (united) atoms. The third term describes the three-body bending interaction with $\Theta_{i,i+1,i+2}$ being the bending angle between the atoms $i,i+1,i+2$. The four-body bonded interaction, giving the internal torsional vibrations, is expressed in (4) with $\tau_{i,i+1,i+2,i+3}$ representing the torsional angle between the atoms $i,i+1,i+2,i+3$. The interaction between any two nonbonded atoms is described by a Lennard-Jones potential in (5). The cutoff parameter for the nonbonded interaction was 1.0 nm, and N is the number of atoms. The parameters for (1)–(5) are listed in Table 1 [16, 18–20].

The Lagrangian equations of motion

$$\frac{\partial L}{\partial q_j} - \frac{\mathrm{d}}{\mathrm{d}t}\frac{\partial L}{\partial \dot{q}_j} = 0 \qquad j = 1, 2, \ldots\ldots, s \tag{6}$$

Table 1 Model parameters

Two-body interactions	Four-body interactions
D = 334.72 kJ mol^{-1}	a = 18.41 kJ mol^{-1}
r_e = 0.153 nm	b = 26.78 kJ mol^{-1}
α = 19.9 nm^{-1}	
Three-body interactions	Nonbonded interactions
K_Θ = 130.22 kJ mol^{-1}	ε = 0.477 kJ mol^{-1}
Θ_0 = 113°	σ = 0.398 nm

were then solved on a CRAY-XMP computer at Oak Ridge National Laboratory. For further information on the technique see references [21–23].

Result

Several simulation runs were used for the discussion in this paper. Their code, length of time and initial temperature are listed in Table 2.

Table 2 Run parameters

Run Code	Time/ps	Initial T/K
D01	10	65
D02	10	165
D03	10	242
D04	10	345
D05	100	436

To create the temperature for the simulation, a randomly distributed set of momenta was given to the atoms. The temperature was then calculated after various times of motion according to

$$\frac{3}{2}N k_B T = \frac{1}{2}m \sum_{i=1}^{N} (\dot{x}_i^2 + \dot{y}_i^2 + \dot{z}_i^2) \tag{7}$$

with k_B being Boltzmann's constant.

Due to the cutoff of the nonbonded interaction at 1 nm, the integrator lost energy [24]. This energy loss is equivalent to a cooling rate of approximately 0.8 K ps^{-1} and sufficiently slow to keep the system thermally in steady state. The range of the run D05 was chosen to cover the melting point of paraffins with a length of 50 carbon atoms, which is about 365 K [25]. Figure 2 displays

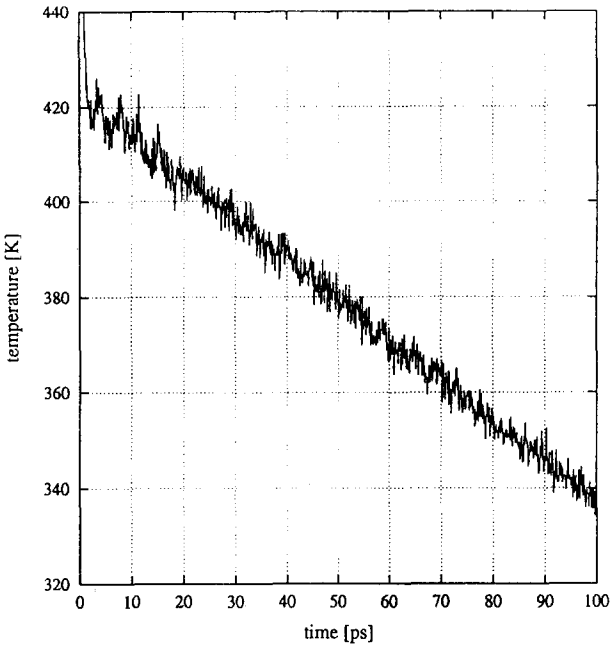

Fig. 2 Temperature during run D05 as a function of time (cooling curve)

the temperature decrease of run D05. Similar, but shorter curves describe the other runs.[3] The simulations allow thus to establish a typical 'cooling curve'.

Since the total energy of the system is also available at any instant, the energy *vs.* time and temperature *vs.* time curves could be combined, as shown in Fig. 3. A more detailed view is presented in Fig. 4. The energies are given in kJ mol^{-1} of united atoms.

The changes in energy and in temperature permit the calculation of heat capacities[4] according to

$$C = \frac{\langle E_1 \rangle - \langle E_2 \rangle}{\langle T_1 \rangle - \langle T_2 \rangle} \tag{8}$$

As was shown earlier [13], thermal equilibrium is achieved in about 2 to 3 ps. For the short time simulations, the averaged energy differences and aver-

3 The temperature changes of the short-time simulations are small, so that, for less temperature-sensitive investigations, the corresponding systems were assumed to be at constant temperature.

4 The heat capacity of Eq. (8) is simulated at constant pressure, similar to the experimental measurements. All compiled heat capacities derived from vibrational spectra are at constant volume and are converted to C_p using standard thermodynamic equations.

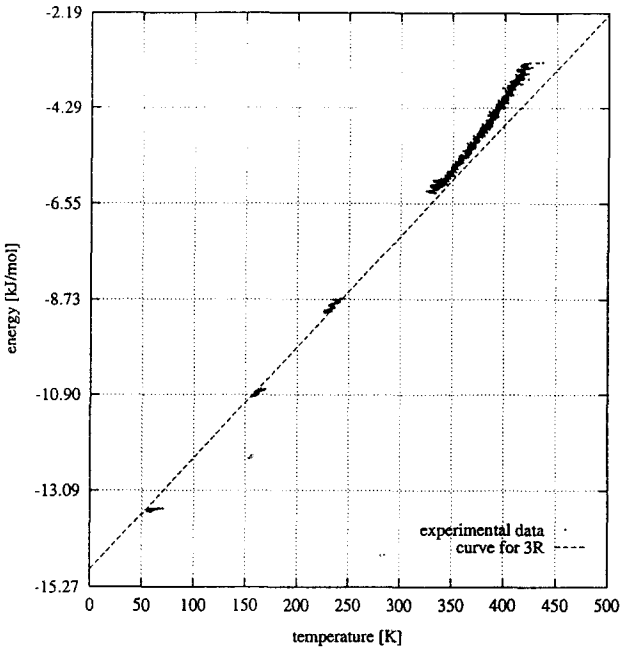

Fig. 3 Energy loss *vs.* temperature from runs D01–D05. The plotted line represents the expected energy loss according to Dulong Petit for a classical solid state ($C=3NR$)

aged temperature differences were therefore taken from the last 6 ps of the simulations. For the 100 ps run (D05), which overlaps with run D04, two values were calculated, one for the high temperature regime and one for the low temperature regime. The resulting heat capacities are plotted in Fig. 5. The error bars indicate the uncertainty solely due to the geometric averaging process.[5]

Discussion

Before discussing the results, one needs to briefly review the basics of heat capacity in the solid state. The storage of heat in a solid can only be understood if one uses quantum mechanics. Essential is that energy, in this case thermal energy, can only be added to a system if the amount is big enough to carry the system from its ground state to at least its first excited level. This is the reason why all heat capacities go to zero when the temperature is approaching zero (kelvin). Even if the thermal energy is comparable to or larger than the separation of the

5 Note that the values resulting from this procedure are better than expected from Fig. 4.

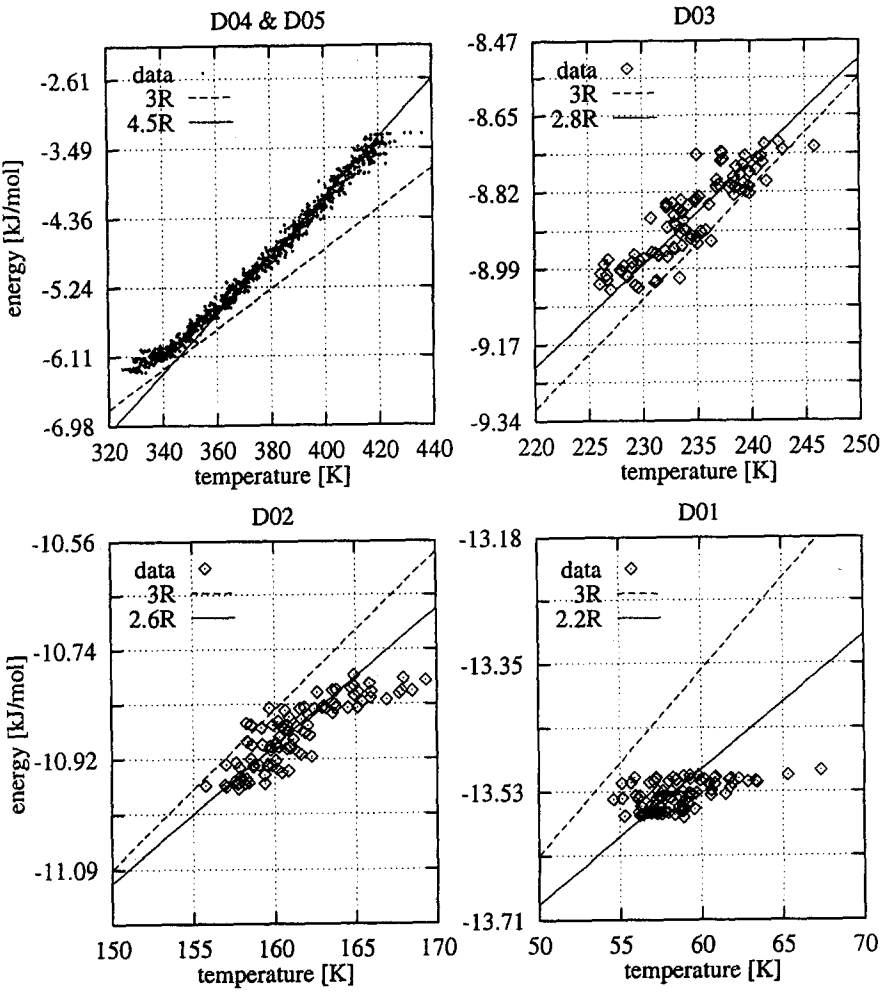

Fig. 4 Energy loss *vs.* temperature for single runs. Included are the 3*R* line from Fig. 3 (dashed lines) and the curves corresponding to the obtained values of Fig. 5 (drawn out)

energy levels, limitations apply. Considering, as an example, a system made of uncoupled harmonic oscillators with the same frequency (Einstein model), one can easily deduce the heat capacity.[6]

6 Note that for moderate temperatures, the difference between C_V and C_P is in the percentage range and is not of importance for the following qualitative discussion.

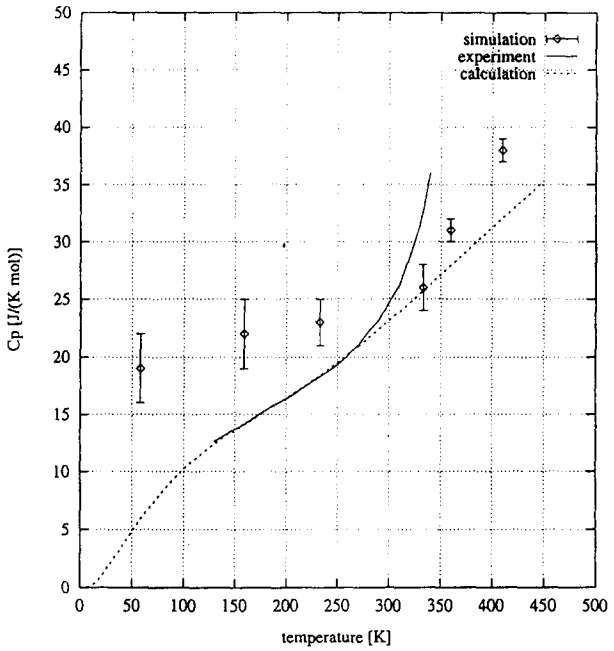

Fig. 5 Heat capacity C_p *vs.* temperature, deduced from the runs D01–D05. Included are experimental results from Jin [26] and calculated data using the ATHAS databank system [27, 28]

$$C_v = R \cdot \frac{\left(\frac{\Theta}{T}\right)^2 \exp\left(\frac{\Theta}{T}\right)}{\left(\exp\left(\frac{\Theta}{T}\right) - 1\right)^2} \tag{9}$$

with $\Theta = \hbar\omega/k_B$ and the difference in energy level equal to $k_B\Theta$. Equation (9) is displayed in Fig. 6 for different Θ-temperatures. The curves show the contribution of an oscillator of given frequency to the heat capacity as a function of temperature. It can be seen clearly that oscillators with high frequencies do not contribute very much to the heat capacity in the temperature range where polymers are used. Every oscillator can accept the same amount of energy, namely $R = 8.314$ J (K mol)$^{-1}$, only if the thermal energy is much larger than the difference in energy levels.

Classical mechanics states in contrast, that each oscillator contributes $1R$ to the heat capacity regardless of temperature. A continuous increase of the amplitude of motion is possible at any temperature. Overall each energy term for a generalized coordinate which has a quadratic dependency in the coordinate con-

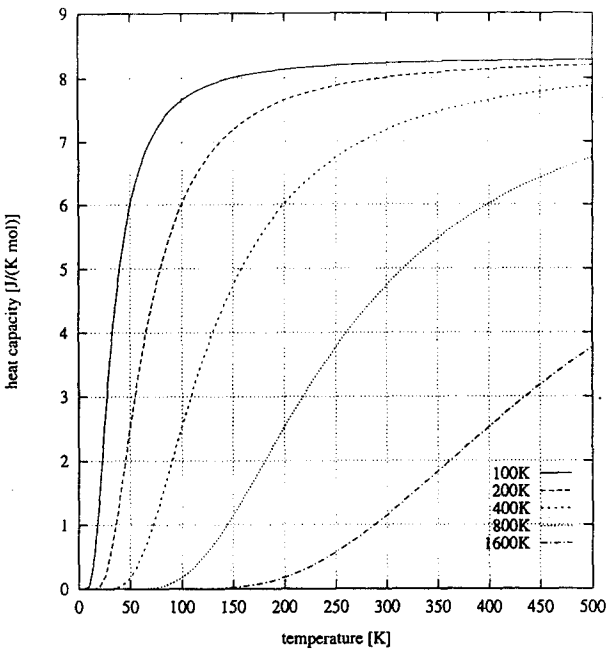

Fig. 6 Calculated heat capacity for the Einstein model for different Θ-temperatures according to Eq. (9)

tributes $R/2$ to the heat capacity. This is known as the equipartition theorem. In this respect an oscillator has two $R/2$ contributions, a kinetic one and a potential one. This also implies that there are deviations if the dependency on the coordinate is not quadratic. Looking at Eqs (1) to (5), it is obvious that only the kinetic energies and the bending term should deliver $R/2$. All other parts are anharmonic, having an upper limit in binding energies. The influence of the anharmonicities on a single linear chain was investigated by Sumpter, Noid and Wunderlich [29]. The result was that the contribution to the heat capacity decreases slightly at higher temperatures. There is an easy way to qualitatively understand this effect. Consider as an example the limiting heat capacity for a particle in such an open potential in one dimension (for example a Morse potential that is limited in the direction of large bond length due to dissociation). For low temperatures, the anharmonicity can be neglected, the particle is an oscillator contributing $1R$. At high temperatures, the particle will dissociate from the restricting potential and contributes as a free particle only the kinetic energy, i.e. $R/2$. This means that approaching dissociation, the anharmonicity leads to a reduction in the contribution to the heat capacity. One can get the same result from the following argument. What is heat capacity? It measures the changes in energy due to changes in temperature. What is temperature? Ac-

cording to the kinetic gas theory, it can be connected to the kinetic energy. We used these definitions to evaluate the temperature in the simulations. So, in a first step an increase in temperature will lead to an increase in kinetic energy, meaning vibrational velocity.[7]

This increased velocity will also increase the amplitude of motion in our potential. If the potential is harmonic, a constant increase in potential energy results, irrespective of the amplitude. But in case of a Morse potential, the increase in amplitude will give decreasing changes in potential energy. Ultimately the potential energy will stop increasing at the top level of the potential (dissociation). This discussion is readily transferred to quantum mechanics. A quantitative discussion can be found in the Appendix.

But, as long as the temperatures are not large, which is true for the presented simulations, the deviations are small.

Additional informations concerning the problem quantum mechanics versus classical mechanics can be found in an article by Lacks and Rutledge [30]. They compare in great detail lattice parameters, moduli, Gruneisen parameters and expansion coefficients, derived through quantum mechanical and classical calculations using a quasi-harmonic approach.

Figure 3 shows that the overall heat capacity is close to $3R$, as expected from the chosen classical molecular dynamics simulation with united atoms. Each united atom has initially six degrees of freedom, three in position and three in velocity. In the solid state this leads to three vibrational degrees of freedom. As each oscillator contributes $1R$ in heat capacity, the classical heat capacity is $3 \cdot 1R = 3R$. A closer look at Figs 4 and 5 reveals, however, deviations from $3R$ in the lower temperature range as well as in the upper range. The deviations in the lower range may be due to several reasons. First, the simulation time could be too short. Despite being thermally in equilibrium, energy changes due to diminishing volume fluctuations [31] in the first ten to twenty picoseconds may conceal a heat capacity contribution. Another possibility is the following. As long as the temperature is relatively high, the weak perturbation due to the nonbonded interaction (Eq. (5)) can be neglected. At low temperature, however, the influence becomes stronger and the intermolecular interaction slows the vibrational motions. This is comparable to a weakening of the vibrational potential and is anharmonic due to the Lennard-Jones potential (Eq. (5)). In analogy to the anharmonic effects discussed earlier, this should lead to a decrease of heat capacity.

7 To be precise, the kinetic energy also includes rotational and translational parts. If they give rise for an ordered macroscopic movement, for example a translation of the center of mass, these contributions must be excluded for the temperature calculation. In the presented simulations this could be neglected.

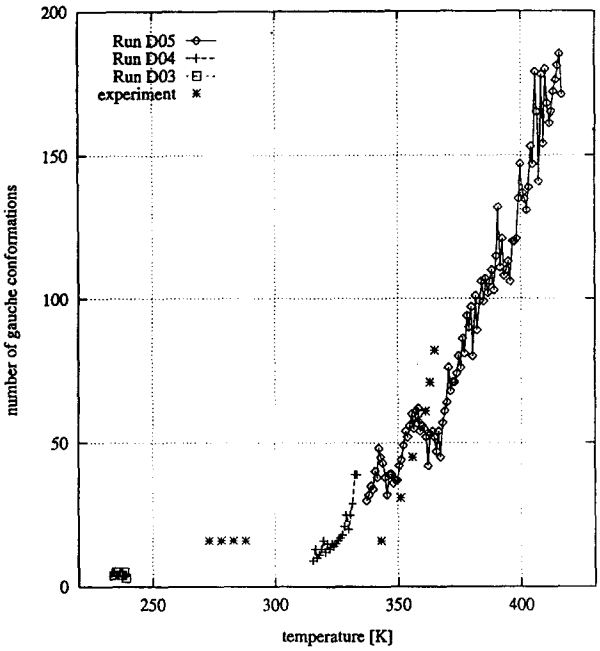

Fig. 7 Number of gauche conformations *vs.* temperature from runs D03–D05. Included are adjusted experimental results form Kim, Strauss and Snyder [35]. The total number of bonds available for rotation is 9216

Nevertheless, it must be clearly stated that in the low-temperature range the quantum mechanical effects limit the usefulness of the classical simulations. Therefore, the difference between the experimental values in Fig. 5 and the simulated data cannot be related to any specific cause in the simulation, even though the united atom model is a good approximation for paraffins or polyethylene in most of the temperature range. A normal mode analysis[8] for the CH_2-group of a linear chain (paraffin, polyethylene) (see for example [32]) reveals that only 2, and with lesser precision 3 vibrations are sufficiently excited. These exited vibrations are the torsional- and accordion-like skeletal vibrations, and to a minor extend the C–C stretching mode. The latter couples weakly due to a relatively small deviation from 90 degree of the bond angle. All other group vibrations [32] have a much higher frequency. These three actual vibrations correspond well to the three vibrations of the united atom model.

The positive deviation in the higher temperature regime is more interesting. As discussed above, it cannot be related to anharmonicity, because anharmonic-

8 Note that a normal mode analysis is in itself a harmonic approximation.

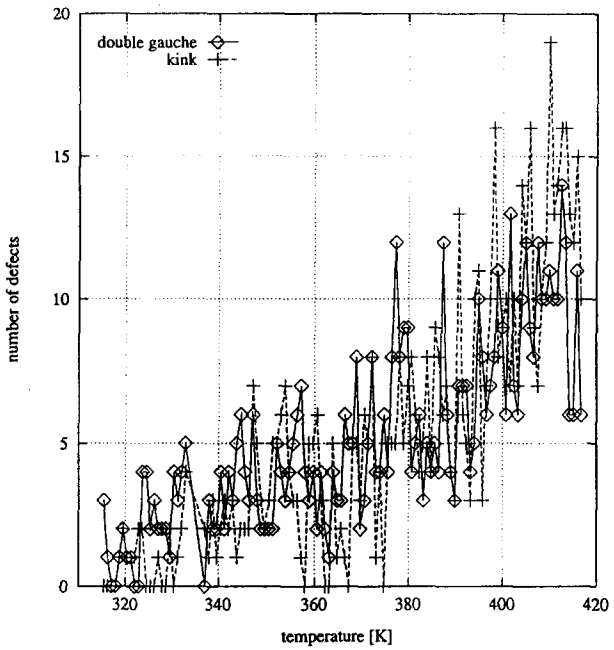

Fig. 8 Number of double gauche-bonds or kink defects *vs.* temperature from runs D04–D05

ity would decrease the heat capacity. Although the contributions of the group vibrations to the experimental heat capacity increase in value beyond $3R$, the calculations using the ATHAS[9] Data bank scheme (see dashed line in Fig. 5) show that there is still an additional positive deviation of the experimental data, also plotted in Fig. 5. The simulated data shows a similar trend, especially when looking at the detailed energy plot (Fig. 4). This added increase in heat capacity has to be a new effect. One possibility is the generation of defects in the crystal at higher temperature. Figure 7 shows the number of gauche conformations formed in the crystal of the 9600 united atoms. The values are in agreement with earlier simulations of smaller systems under constant volume conditions [33, 34]. At the highest temperature the maximum percentage reaches about 2% of gauche conformations. Infrared measurements of Kim, Strauss and Snyder [35] (see * in Fig. 7) support the generation of such an amount of gauche defects. Larger defects, like double gauche-bonds or 2g1-kinks were detected only infrequently (cf. Fig. 8). The percentage is about 0.2%. The onset of the increase in gauche defects can be found at the same tem-

9 Advanced Thermal Analysis System, see for example Refs [27, 28].

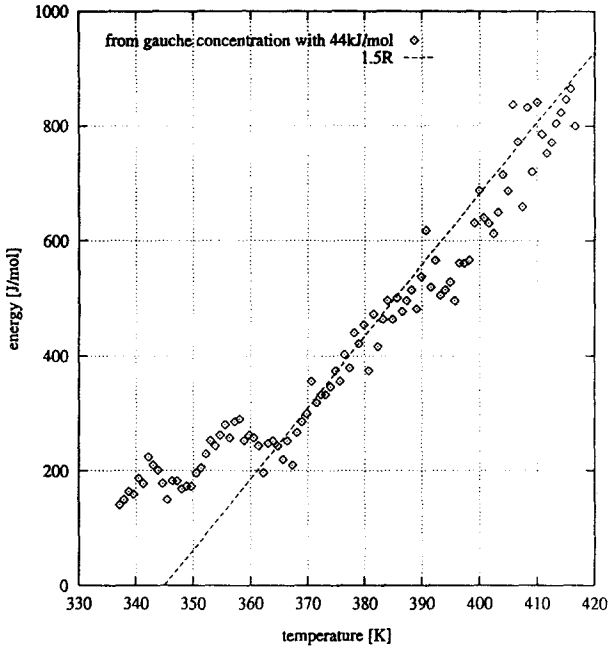

Fig. 9 Calculated energies from simulated gauche defect numbers assuming an energy of 44 kJ/(mol of defects) *vs.* temperature. The 1.5*R* fit from Fig. 4 for the high temperature was taken as comparison line

perature where the heat capacity increases more steeply to a higher value. In the same temperature region a 'transition' from a more rigid, low-temperature phase to a more mobile (hexagonal) rotator-like phase could be detected [31, 36]. This finding supports a distinct increase in the disordering in the temperature regime below the melting point.[10] Assuming that most of the extra heat capacity is due to the defects, one can deduce from the increase in heat capacity of about 1.5*R* (cf. Fig. 9), a contribution of about 44 kJ mol^{-1} of defects. This can be compared to the energy difference between trans and gauche conformations of 3.3 kJ mol^{-1} in polyethylene. Clearly, about 90% are coming from other causes, when forming a defect. As most defects are simple gauche conformations, this indicates that defect creation is a cooperative effect. Reneker and Mazur [37] calculated several low-energy defect types with molecular mechanics. Although molecular mechanics suffers from its static treatment, the obtained values are in the same energy range, for example chain twist boundary

10 Note that due to the short overall simulation time of 100 ps a macroscopic melting during the simulation is not possible. The simulated crystal is superheated at temperatures above about 365 K. This extends the regime where the disordering can be observed.

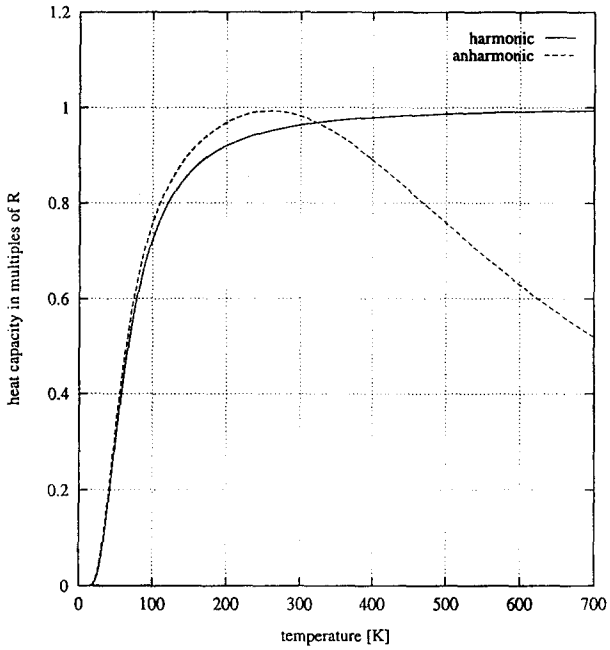

Fig. 10 Calculated heat capacity for a Morse potential in comparison with a harmonic potential. The heat capacity is given in multiples of R. (For parameters used in the computation, see Text)

(90°) 32.7 kJ mol^{-1}, disclinations 72.1 kJ mol^{-1}, and interstitial-like dispiration 49.2 kJ mol^{-1}. But all of these calculated defects are more complex than the simple gauche defects, that dominate our dynamic simulation.

Conclusion

In this paper it is shown that it is possible to simulate thermal analysis using molecular dynamics. However, one must be aware of the limitations due to the excitation probability of quantum mechanical vibrators. In this respect a united atom model is a good choice because two of the three modes of vibration resemble the two almost fully excited solid state vibrations in paraffin or polyethylene at room temperature. The third mode (united atom stretching) can be associated with the C–C stretching vibration which is at least partially excited, and the combined contribution of all other group vibrations. A full atom simulation would lead to overestimated vibrational contributions since the C–H bending and stretching vibrations have Θ-temperatures above 2000 K and contribute little to heat capacity at room temperature. This is especially critical for thermal analysis, but may also explain some deviations in other properties. In the future,

an incorporation of the implications of Fig. 6 into the classical molecular dynamics simulation would improve the results. For the heat capacity, anharmonicity as well as the generation and influence of defects were also investigated. While aharmonicity decreases the heat capacity, defects tend to show an increase. The melting of a polymer crystal, which has to start from the surface, seems to be preceeded by a generation of point defects, which contribute a significant amount to the heat capacity of the crystal. The defects are mainly simple gauche conformations, generated cooperatively with other energy consuming processes (local strain energy).

* * *

This work was supported by the Division of Materials Research, National Science Foundation, Polymers Program, Grant # DMR 92-00520 and the Division of Materials Sciences, Office of Basic Energy Sciences, U.S. Department of Energy, under Contract DE-AC05-84-OR21400 with Martin Marietta Energy Systems, Inc.

SNK and GLL wish to express their deep gratitude towards Prof. Wunderlich for his continuous and fruitful discussions about thermal analysis and molecular dynamics. SNK wishes to thank the Alexander-von-Humboldt Foundation for its partial support of his stay at the University of Tennessee Knoxville.

The submitted manuscript has been authored by a contractor of the U.S. Government under contract No. DE-AC05-84OR21400. Accordingly, the U.S. Government retains nonexclusive, royalty-free license to publish or reproduce the published form of this contribution, allow others to do so, for U.S. Government purposes.

Appendix

In this appendix the influence of anharmonicity of a Morse potential on the heat capacity is shown in a quantum mechanical treatment.[11] As Morse could show, the Schrödinger equation with the so called Morse potential

$$\left(\frac{\hbar^2\nabla^2}{2\mu} - D(1 - \exp(-\alpha(r - r_o))^2\right)\Psi = E\Psi$$

can be solved analytically, μ being the reduced mass of the particle in the potential, D, the dissociation energy, r_o, the equilibrium distance, and α, a measure of the stiffness of the potential. The resulting energy levels are

$$\varepsilon_n = \hbar\omega(n + 1/2) - x\hbar\omega(n + 1/2)^2$$

with ω being an effective frequency and x, the anharmonicity parameter. All of them are related to the parameters of the potential. Introducing the Θ-tempera-

11For further information refer to Herzberg [38].

ture $\Theta = \hbar\omega/k_B$ and neglecting the zero point energy one gets for the partition function

$$Q = \sum_{n=1}^{m} e^{-\frac{\varepsilon_n}{k_B T}} = \sum_{n=1}^{m} e^{\frac{-(1-x)\Theta n + x\Theta_n^2}{T}}$$

m being the finite number of energy levels in the Morse potential. Using

$$E = RT^2 \frac{\mathrm{d}\ln Q}{\mathrm{d}T}$$

the internal energy is

$$E = R \cdot \Theta \cdot \left\{ \sum_{n=1}^{m} ((1-x)\, n - xn^2)\, e^{\frac{-(1-x)\Theta n + x\Theta n^2}{T}} \right\} \Big/ \left\{ \sum_{n=1}^{m} e^{\frac{-(1-x)\Theta n + x\Theta n^2}{T}} \right\}$$

With the definition of the heat capacity

$$C_v = \frac{\mathrm{d}E}{\mathrm{d}T}$$

the final result is

$$C_v = R \cdot (\Theta/T)^2 \cdot$$

$$\left(\left\{ \sum_{n=1}^{m} ((1-x)\, n - xn^2)^2\, e^{\frac{-(1-x)\Theta n + x\Theta n^2}{T}} \right\} \Big/ \left\{ \sum_{n=1}^{m} e^{\frac{-(1-x)\Theta n + x\Theta n^2}{T}} \right\} - \right.$$

$$\left. - \left\{ \sum_{n=1}^{m} ((1-x)\, n - xn^2)^2\, e^{\frac{-(1-x)\Theta n + x\Theta n^2}{T}} \right\} \Big/ \left\{ \sum_{n=1}^{m} e^{\frac{-(1-x)\Theta n + x\Theta n^2}{T}} \right\}^2 \right)$$

The following plot, Fig. 10, shows C_v *vs.* temperature. As example we took 0.01 for x, Θ=200 K, and 12 energy levels. It can be seen that in the low temperature regime, there is a close similarity to the harmonic solution. For high temperatures the heat capacity of the Morse potential starts to decrease. In a real system there would be a continuous energy band above the Morse potential, representing the free state. Therefore the decrease will not go to zero, as in this calculation, but will stop at $R/2$, the heat capacity for a free particle moving in one dimension.

References

1 D. N. Theodorou and U. W. Suter, Macromolecules, 19 (1986) 139.
2 S. Kreitmeier, M. Wittkop and D. Göritz, J. Comp. Phys., 112 (1994) 267.

3 A. Baumgärtner, J. Chem. Phys., 73 (1980) 2819.
4 I. Carmesin and K. Kremer, Macromolecules, 21 (1988) 2819.
5 J. J. De Pablo, M. Laso and U. W. Suter, J. Chem. Phys., 96 (1992) 2395.
6 M. Wittkop, J.-U. Sommer, S. Kreitmeier and D. Göritz, Phys. Rev. E., 49 (1994) 5472.
7 A. Baumgärtner and K. Binder, J. Chem. Phys., 75 (1981) 2994.
8 M. Bishop, D. Ceperley, H. L. Frisch and M. H. Kalos, J. Chem. Phys., 72 (1980) 3228.
9 T. A. Kavassalis and P. R. Sundararajan, Macromolecules, 26 (1993) 4144.
10 D. Rigby and R. J. Roe, Macromolecules, 22 (1989) 2259.
11 D. W. Noid, B. G. Sumpter and B. Wunderlich, Macromolecules, 23 (1990) 664.
12 D. W. Noid, B. G. Sumpter and B. Wunderlich, Macromolecules, 24 (1991) 4184.
13 G. L. Liang, D. W. Noid, B. G. Sumpter and B. Wunderlich, J. Polymer Sci.: Part B Polymer Phys., 31 (1993) 1909.
14 G. L. Liang, D. W. Noid, B. G. Sumpter and B. Wunderlich, Makromol. Chem., Theory Simul., 2 (1993) 245.
15 C. W. Bunn, Trans. Farad. Soc., 35 (1939) 482.
16 B. G. Sumpter, D. W. Noid and B. Wunderlich, Macromolecules, 25 (1992) 7247.
17 D. W. Noid, B. G. Sumpter and B. Wunderlich, Anal. Chim. Acta, 235 (1990) 143.
18 B. G. Sumpter, D. W. Noid, B. Wunderlich and S. Z. D. Cheng, Macromolecules, 23 (1990) 4671.
19 R. H. Boyd and S. M. Breitling, Macromolecules, 7 (1974) 855.
20 D. Brown and J. H. R. Clarke, J. Chem. Phys., 84 (1986) 2858.
21 D. W. Noid, B. G. Sumpter, B. Wunderlich and G. A. Pfeffer, J. Comp. Chem., 11 (1990) 236.
22 L. F. Shampine and M. K. Gordon, Computer solutions of ordinary differential equations: the initial value problem, Freeman, San Francisco 1975.
23 G. L. Liang, D. W. Noid, B. G. Sumpter and B. Wunderlich, Comput. Poly. Sci., 3 (1993) 101.
24 G. L. Liang, D. W. Noid, B. G. Sumpter and B. Wunderlich, Acta Polymer., 44 (1993) 219.
25 M. G. Broadhurst, J. Res. Natl. Stand., 66A (1962) 241.
26 Y. Jin and B. Wunderlich, J. Phys. Chem., 95 (1991) 9000.
27 Yu. V. Cheban, S.-F. Lau and B. Wunderlich, Coll. & Polymer Sci., 260 (1982) 9.
28 M. Varma-Nair and B. Wunderlich, J. Phys. Chem. Ref. Data, 20 (1991) 349.
29 B. G. Sumpter, D. W. Noid and B. Wunderlich, Polymer, 31 (1990) 1254.
30 D. J. Lacks and G. C. Rutledge, J. Chem. Phys., 98 (1994) 1222.
31 S. N. Kreitmeier, G. L. Liang, D. W. Noid and B. Wunderlich, Polymer International, 36 (1995) 155.
32 B. Wunderlich, Thermal Analysis, Academic Press, New York, London, Toronto, Sydney, San Francisco 1990.
33 B. G. Sumpter, D. W. Noid and B. Wunderlich, J. Chem. Phys., 93 (1990) 6875.
34 D. W. Noid, B. G. Sumpter, M. Varma-Nair and B. Wunderlich, Makromol. Chem., Rapid Commun., 10 (1989) 1989.
35 Y. Kim, H. L. Strauss and R. G. Snyder, J. Chem. Phys., 93 (1989) 7520.
36 S. N. Kreitmeier, G. L. Liang, D. W. Noid and B. Wunderlich, J. Chem. Soc. Faraday Trans., 91 (1995) 2601.
37 D. H. Reneker and J. Mazur., Polymer 29 (1988) 3.
38 G. Herzberg, Molecular Spectra and Molecular Structure, D. Van Nostrand Company, Princeton NJ, Toronto, New York, London 1950.